McKenzie, J.A., Davies, P.J., Palmer-Julson, A., et al., 1993
Proceedings of the Ocean Drilling Program, Scientific Results, Vol. 133

12. THE STABLE OXYGEN ISOTOPE SIGNAL IN SHALLOW-WATER, UPPER-SLOPE SEDIMENTS OFF THE GREAT BARRIER REEF (HOLE 820A)[1]

F.M. Peerdeman,[2] P.J. Davies,[3] and A.R. Chivas[2]

ABSTRACT

Oxygen-isotope ratio measurements are presented for the planktonic species *Globigerinoides ruber* collected from shallow-water, upper-slope sediments from Holes 820A and 820B in 280 m of water, on the seaward edge of the Great Barrier Reef. Correlation of the Site 820 isotope curve with deep-sea reference curves of the Pacific Ocean (Core V28-238, Hole 677A, Hole 607A) permits the definition of isotope stages 1 to 19 in the top 145 m of Holes 820A and 820B. However, paleontological data indicate that stages 4 and 7 might be missing and that two hiatuses occur at a depth of 8.05 to 12.1 and 34.55 to 35.8 mbsf. Using deep-sea Hole 677A as a reference for ice-volume variations, we determine the difference in isotopic signature between it and Site 820. We propose that this difference is a regional signal representing a progressive 4°C increase in surface-water temperature at Site 820. The proposed temperature change was initiated at about 400 k.y. and corresponds to a change from high-to-low frequency variations in Pleistocene isotope signals. We postulate that these changes may have catalyzed the growth of the Great Barrier Reef. The shift also coincides with changes in seismic character and some physical and chemical sediment characteristics.

INTRODUCTION

Since the innovative work of Shackleton and Opdyke (1973) and Broecker (1974), oxygen-isotope signals in deep-sea cores have been used both to define a Pliocene–Pleistocene stratigraphy at scales of thousands to hundreds of thousands of years and to invoke climatic and sea-level oscillations in the Quaternary and late Cenozoic (Ruddiman et al., 1989; Shackleton and Hall, 1989). Comprehensive oxygen-isotope curves have been established for the Pliocene and Pleistocene from deep-sea records that indicate fluctuations in global ice volume, which are generally accepted as approximating changes in sea level (Chappell and Shackleton, 1986). Detailed spectral analyses of these deep-sea isotope records also indicate that the mode of isotopic change has varied with time, such that high-frequency, low-amplitude variations dominated between 2.47 and 0.735 Ma, while low-frequency, high-amplitude variations dominated since 0.735 Ma (Prell, 1982; Imbrie, 1985; Imbrie et al., 1984; Ruddiman et al., 1986, 1989; and Maasch, 1988). Invariably, most published studies have emphasized the completeness and the high-resolution nature of the deep-sea record.

In spite of the fact that accumulation rates on continental shelves and slopes have the potential to produce a far higher resolution record than those in the deep sea, few have attempted to define a coherent isotope signal from such environments. The conventional arguments against the utility of such environments are that (1) the sedimentation rates vary substantially between intervals of high and low sea level; (2) hiatuses are common, and (3) bioturbation may destroy or downgrade any potential signals. Here, we examine such suggestions by defining an isotope signal for the late Quaternary, the resolution of which is equal to or greater than that found in deep-sea signals. These data were obtained from Holes 820A and 820B in 280 m of water on the upper slope of the Great Barrier Reef (Fig.1).

Earlier studies in the region defined the seismic structure of the continental slope in front of the outer reefs of the Great Barrier Reef (Davies et al., 1988, 1989; Feary et al., 1990). Part of the seismic data set on which the drilling was based is presented in Figure 2, which shows a west-to-east line, for which our pre-drilling scenario emphasized (1) an extremely high-resolution section in the top 80 m (approximately 500 ms), thought to represent the late Pleistocene; (2) a large-scale change in geometry from prograding to aggrading (approximately 560 ms), thought to relate to global climate changes around the Brunhes/Matuyama boundary; and (3) a seismic character for the aggrading section that suggested cyclic lithologic changes tied to sea level and climatic oscillations (Harris et al., 1990).

Lithologic analyses performed on board the *JOIDES Resolution* together with determinations of $CaCO_3$ variations, whole-core magnetic susceptibility, and physical property measurements combined with paleontological age determinations substantiate these conclusions and underlie our rationale for sampling Holes 820A and 820B at closely spaced intervals. This rationale emphasizes the establishment and use of a high-resolution, stable oxygen-isotope signal in reference to a deep-sea isotope record to relate lithological, sedimentological, and large-scale seismic geometric changes on the slope of the Great Barrier Reef to fluctuations in glacio-eustatic sea level and paleoclimatic changes. Site 820 was drilled to a depth of 400 m and bottomed at an age of less than 1.4 Ma. Therefore, it represents an extremely high-resolution section for the middle and late Pleistocene.

METHODS

Sampling densities throughout Holes 820A and 820B were typically one sample every 20 cm, with the exception of the section from 130.75 to 121.5 mbsf in Hole 820A, in which a poorly sorted bioclastic wackestone to floatstone, underlain by an unconsolidated clayey wackestone, did not allow for regular sampling intervals.

From each sample, 10 specimens of *Globigerinoides ruber* were carefully hand-picked from the 250- to 350-µm fraction. Each set of foraminifers was cleaned in Milli-Q(TM) ultra-pure H_2O by using an ultrasonic bath for approximately 1 min to remove fine-fraction contamination. The water was then siphoned off with a pipette, and the foraminifers rinsed over a 125-µm nylon mesh, again with Milli-Q water. After inspecting the foraminifers for internal contamination in translucent light, we analyzed stable oxygen isotopes of the calcitic foraminifers at the stable-isotope laboratory of the Research School of Earth Sciences of the Australian National University. For this, we used an automated "acid-on-individual carbonate" (or Kiel) preparation device attached to a Finnigan MAT 251 mass-spectrometer. Analyses are expressed as per mil deviation (δ) from the PDB standard (Epstein et al., 1953).

1 McKenzie, J.A., Davies, P.J., Palmer-Julson, A., et al., 1993. *Proc. ODP, Sci. Results,* 133: College Station, TX (Ocean Drilling Program).

2 Research School of Earth Sciences, The Australian National University, Canberra ACT 0200, Australia.

3 Department of Geology and Geophysics, University of Sydney, Sydney NSW 2006, Australia.

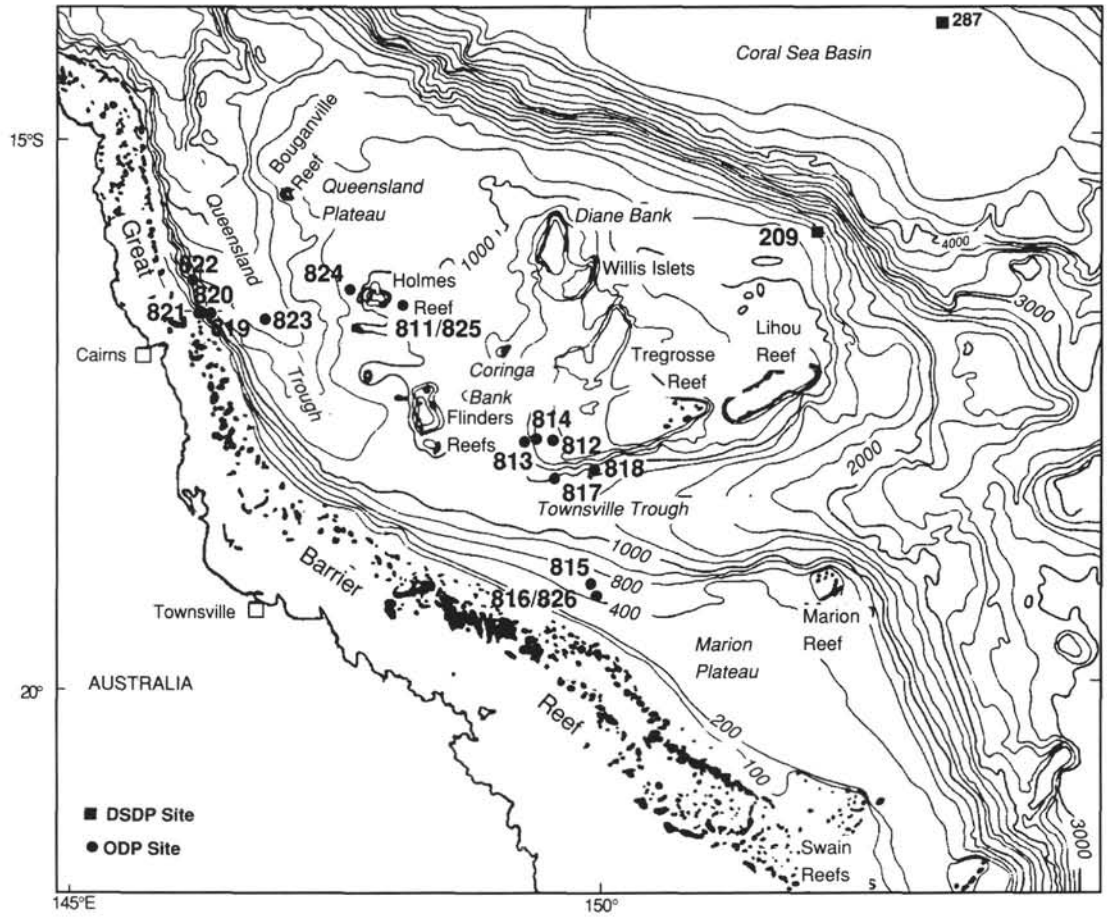

Figure 1. Locality map showing the principal bathymetric features of the northeastern Australian continental margin and the position of Site 820 east of Cairns.

Analytical precision of the working standard (M-2 Bulk, 1991) reached during the measurements was 0.02‰ (2σ). Reproducibility of solid NBS-19 standard (approximately 160 measurements, each on ±150 µg of $CaCO_3$), is 0.05‰.

INTERHOLE CORRELATION

Hole 820A was cored approximately 20 m east of Hole 820B (Davies et al., 1991). Samples presented here were collected from the upper 140.15 mbsf of Hole 820A and from 131.95 to 148.48 mbsf in Hole 820B. In matching features and absolute $\delta^{18}O$ values of both holes, we used the oxygen-isotope signal as a convenient means of transforming depths of Hole 820B to those of 820A, within the overlapping section. This is done by adding 2.2 m to sample depths from Hole 820B, to provide the equivalent depth at Hole 820A. The adjusted depths of samples from Hole 820B can be found in Table 1 under the heading "adj. dbsf." Likewise, when using the magnetic susceptibility data from both holes, Barton and others (this volume) found Site 820 to contain a most satisfactory record for interhole correlation. On that basis, they have compared both holes (820A and 820B) to an accuracy generally within 20 cm. Barton and others find a similar offset of approximately 2.2 m in both holes at ~120 to 140 mbsf.

RESULTS

The $\delta^{18}O$ values of the planktonic foraminifer *G. ruber* for Holes 820A and 802B are listed in Table 1 and presented in Figure 3. The results show a well-defined, high-resolution cyclic behavior of $\delta^{18}O$, with a maximum variability of 1.9‰. The overall signal ranges from –2.6‰ at the top of the hole to +0.4‰ at the bottom.

A distinct change in the variability of the $\delta^{18}O$ values can be recognized at about 75 mbsf, below which the $\delta^{18}O$ values indicate rapid cyclic variability with overall large amplitudes. Shallower than 75 mbsf, each increasing trend of $\delta^{18}O$ values extends over many meters of rock section. These sections contrast with the intervening decreasing trends of $\delta^{18}O$ values, which occur more abruptly over tens of centimeters of rock section. The high-$\delta^{18}O$ layers also show a high-frequency, low-amplitude (±0.3‰) variability. We caution against any overinterpretation of these minor variations because duplicate measurements from the upper 10 mbsf have indicated that measurements on foraminifers of the same horizon can vary by ±0.13‰ (2σ) with a maximum deviation of 0.38‰ (Table 2). The modern seasonal temperature variations of the surface waters at Site 820 (22 to 27°C: Pickard, 1977) can readily account for these small fluctuations in $\delta^{18}O$.

AGE MODELS

We offer two possible age models for the data shown in Figure 3. Our first interpretation, presented in Figure 4A, is based on a comparison of the oxygen-isotope data from Holes 820A and 820B with records obtained from the western equatorial Pacific deep-sea Core V28-238 (Shackleton and Opdyke, 1973) and from the eastern Pacific Hole 677A (Shackleton and Hall, 1989). The reasons for comparing Holes 820A and 820B with Core V28-238 and Hole 677A are that (1) all sites lie in the tropical zone of the equatorial Pacific, (2) all sites contain oxygen-isotope information that primarily reflects changes in

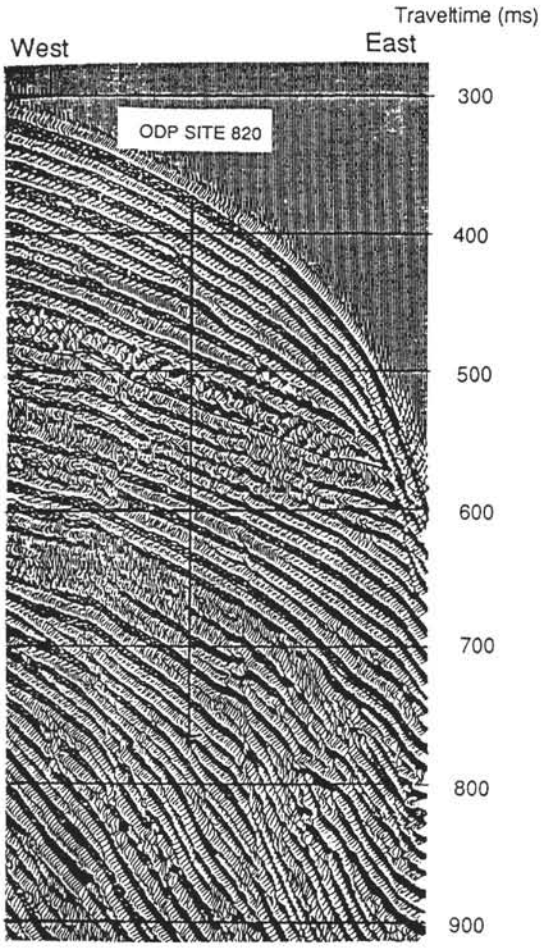

Figure 2. Seismic data through Site 820 on a west-to-east transect off the Great Barrier Reef, east of Cairns.

ice volume (Shackleton and Opdyke, 1973), and (3) Core V28-238 and Hole 677A together contain a complete and relatively detailed $\delta^{18}O$ stratigraphy for the Pleistocene and uppermost Pliocene. Each of the three core sections has a high, uniform sedimentation rate that is likely to result in $\delta^{18}O$ values that have been little perturbed by sediment mixing.

Our first age model was established by using the graphic correlation concepts outlined by Prell et al. (1986). Correlation was based on a sequential numerical taxonomy of isotope stratigraphy that incorporated not only 19 stage boundaries (defined by Emiliani, 1955, and Shackleton and Opdyke, 1973), but also 56 isotopic events within individual stages. All stage boundaries and almost every interstadial isotopic event (as outlined by Prell et al., 1986) have been identified and were assigned the correct numerical coding (Fig. 4A). On this basis, we conclude that the upper 145 m of Site 820 display the first 19 oxygen-isotope stages. Table 3 indicates the depths below seafloor at Site 820 at which we were able to define the recognized stage boundaries. However, a small number of differences in the character of the interstadial isotopic events are seen and these are summarized below.

In Core V28-238, event 3.3 has been defined as the most negative $\delta^{18}O$ value in stage 3. For this reason, we placed event 3.3 at about 20 mbsf in Hole 820A. However, as can be seen in Figure 4A, event 3.3 is followed by at least four other negative events. We defined the uppermost negative event as 3.1 at 8.05 mbsf in Hole 820A, and left the others undefined.

The transition from 8.4 to 9.3 in Core V28-238 is marked by two significant positive (8.6 and 9.2) and three negative (8.5, 9.1 and 9.3) events. We have related these events to the three successive negative

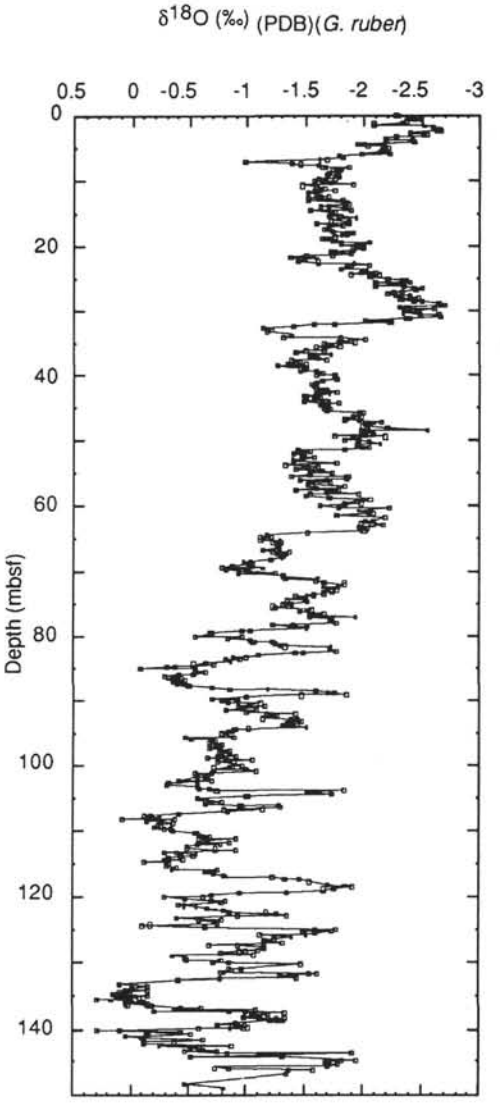

Figure 3. Oxygen-isotopic record for Holes 820A and 820B. The isotopic measurements are for the planktonic foraminifer *Globigerinoides ruber.*

excursions in between 70 and 85 mbsf of Hole 820A. When applying this interpretation, we remark that (1) the increasing trend of $\delta^{18}O$ values in stage 9, as seen in Core V28-238, is not present in Hole 820A, and (2) the transition from 9.3 to 9.1 in 820A is marked by a positive $\delta^{18}O$ excursion (9.2) approximately 0.5‰ heavier than any seen in Core V28-238. We infer that isotope stage 9 and the lower part of stage 8 might contain a secondary regional signal. Likewise, event 11.1 in Hole 820A appears approximately 0.5‰ lighter than that of Core V28-238 and the transition from 11.3 to 12.2 is approximately 0.6‰ less than that observed in Core V28-238. Again, we attribute these differences to a regional effect.

The first model appears consistent with the highest occurrence of *Pseudoemiliania lacunosa* at 107.1 mbsf in Hole 820A (Wei and Gartner, this volume). This datum normally coincides with stages 12/13 (Berggren et al, 1980; Thierstein et al., 1977) and also can be found at the bottom of stage 13 in Hole 820A. The model is also consistent with the revised chronology proposed by Barton and others (this volume), in which the Brunhes/Matuyama boundary has tentatively been placed between 132 and 143 mbsf in Hole 820B (~135 to 145 mbsf in Hole 820A). Our placement of isotope stage 19.1 (generally estimated to be near the Brunhes/Matuyama boundary; DeMenocal et al., 1990) at 145 mbsf is consistent with the interpretation from

Table 1. Oxygen-isotope values of samples of the planktonic foraminifer *G. ruber* from Holes 820A and 820B.

Core, section, interval (cm)	Depth (mbsf)	$\delta^{18}O$
133-820A-		
1H-1, 5–7	0.05	–2.27
1H-1, 25–27	0.25	–2.29
1H-1, 45–47	0.45	–2.38
1H-1, 65–67	0.65	–2.42
1H-1, 85–87	0.85	–2.48
1H-1, 105–107	1.05	–2.37
1H-1, 125–127	1.25	–2.32
1H-1, 145–147	1.45	–2.08
1H-2, 5–7	1.55	–2.08
1H-2, 25–27	1.75	–2.51
1H-2, 45–47	1.95	–2.59
1H-2, 65–67	2.15	–2.64
1H-2, 85–87	2.35	–2.64
1H-2, 93–98	2.43	–2.65
1H-2, 105–107	2.55	–2.63
1H-2, 125–127	2.75	–2.40
1H-2, 145–147	2.95	–2.53
1H-3, 5–7	3.05	–2.54
1H-3, 25–27	3.25	–2.52
1H-3, 45–47	3.45	–2.27
1H-3, 65–67	3.65	–2.18
1H-3, 85–87	3.85	–2.18
1H-3, 93–98	3.93	–2.18
1H-3, 105–107	4.05	–2.41
1H-3, 125–127	4.25	–2.42
1H-3, 145–147	4.45	–1.94
1H-4, 5–7	4.55	–2.00
1H-4, 25–27	4.75	–2.03
1H-4, 45–47	4.95	–2.17
1H-4, 65–67	5.15	–2.20
1H-4, 85–87	5.35	–2.19
1H-4, 105–107	5.55	–2.15
1H-4, 125–127	5.75	–2.13
1H-4, 145–147	5.95	–1.97
1H-5, 5–7	6.05	–2.22
1H-5, 25–27	6.25	–1.77
1H-5, 45–47	6.45	–1.81
1H-5, 65–67	6.65	–1.82
1H-5, 85–87	6.85	–1.62
1H-5, 93–98	6.93	–1.68
2H-1, 5–7	7.25	–0.98
2H-1, 25–27	7.45	–1.37
2H-1, 45–47	7.65	–1.44
2H-1, 65–67	7.85	–1.61
2H-1, 72–77	7.92	–1.65
2H-1, 85–87	8.05	–1.86
2H-1, 105–107	8.25	–1.80
2H-1, 125–127	8.45	–1.74
2H-2, 5–7	8.75	–1.78
2H-2, 25–27	8.95	–1.69
2H-2, 45–47	9.15	–1.67
2H-2, 65–67	9.35	–1.76
2H-2, 85–87	9.55	–1.78
2H-2, 105–107	9.75	–1.75
2H-2, 125–127	9.95	–1.60
2H-2, 145–147	10.15	–1.57
2H-3, 5–7	10.25	–1.65
2H-3, 25–27	10.45	–1.72
2H-3, 45–47	10.65	–1.91
2H-3, 65–67	10.85	–1.47
2H-3, 85–87	11.05	–1.58
2H-3, 105–107	11.25	–1.66
2H-3, 125–127	11.45	–1.57
2H-3, 145–147	11.65	–1.74
2H-4, 5–7	11.75	–1.62
2H-4, 25–27	11.95	–1.53
2H-4, 45–47	12.15	–1.60
2H-4, 65–67	12.35	–1.62
2H-4, 85–87	12.55	–1.69
2H-4, 105–107	12.75	–1.52
2H-4, 125–127	12.95	–1.82
2H-4, 145–147	13.15	–1.52
2H-5, 5–7	13.25	–1.85
2H-5, 25–27	13.45	–1.83
2H-5, 45–47	13.65	–1.87
2H-5, 65–67	13.85	–1.63
2H-5, 85–87	14.05	–1.69
2H-5, 105–107	14.25	–1.83
2H-5, 125–127	14.45	–1.88
2H-5, 141–143	14.61	–1.53
2H-6, 5–7	14.75	–1.71
2H-6, 25–27	14.95	–1.74
2H-6, 45–47	15.15	–1.73
2H-6, 65–67	15.35	–1.69
2H-6, 85–87	15.55	–1.79
2H-6, 105–107	15.75	–1.93
2H-6, 145–147	16.15	–1.71
2H-7, 5–7	16.25	–1.87
2H-7, 25–27	16.45	–1.87
2H-CC, 5–7	16.53	–1.59
3H-1, 25–27	16.95	–1.82
3H-1, 45–47	17.15	–1.69
3H-1, 65–67	17.35	–1.69
3H-1, 85–87	17.55	–1.66
3H-1, 105–107	17.75	–1.72
3H-1, 125–127	17.95	–1.90
3H-1, 143–145	18.13	–1.86
3H-2, 5–7	18.25	–1.81
3H-2, 25–27	18.45	–1.85
3H-2, 45–47	18.65	–1.75
3H-2, 65–67	18.85	–1.64
3H-2, 85–87	19.05	–1.67
3H-2, 105–107	19.25	–1.74
3H-2, 125–127	19.45	–1.80
3H-2, 143–145	19.63	–2.05
3H-3, 5–7	19.75	–1.93
3H-3, 25–27	19.95	–1.80
3H-3, 45–47	20.15	–2.00
3H-3, 65–67	20.35	–1.91
3H-3, 85–87	20.55	–1.98
3H-3, 105–107	20.75	–1.91
3H-3, 125–127	20.95	–1.75
3H-3, 143–145	21.13	–1.71
3H-4, 5–7	21.25	–1.89
3H-4, 25–27	21.45	–1.73
3H-4, 45–47	21.65	–1.49
3H-4, 65–67	21.85	–1.37
3H-4, 85–87	22.05	–1.59
3H-4, 105–107	22.25	–1.47
3H-4, 125–127	22.45	–1.42
3H-4, 143–145	22.63	–1.61
3H-5, 5–7	22.75	–1.91
3H-5, 25–27	22.95	–2.05
3H-5, 45–47	23.15	–1.88
3H-5, 65–67	23.35	–1.85
3H-5, 85–87	23.55	–1.80
3H-5, 105–107	23.75	–1.99
3H-5, 125–127	23.95	–2.00
3H-5, 143–145	24.13	–2.10
3H-6, 5–7	24.25	–1.97
3H-6, 25–27	24.45	–1.89
3H-6, 45–47	24.65	–2.13
3H-6, 65–67	24.85	–2.05
3H-6, 85–87	25.05	–2.21
3H-6, 105–107	25.25	–2.33
3H-6, 125–127	25.45	–2.36
3H-6, 143–145	25.63	–2.39
3H-7, 5–7	25.75	–2.10
3H-7, 25–27	25.95	–2.33
3H-7, 45–47	26.15	–2.09
4H-1, 5–7	26.25	–2.34
4H-1, 25–27	26.45	–2.44
4H-1, 45–47	26.65	–2.50
4H-1, 65–67	26.85	–2.45
4H-1, 85–87	27.05	–2.32
4H-1, 105–107	27.25	–2.25
4H-1, 125–127	27.45	–2.20
4H-1, 145–147	27.65	–2.28
4H-2, 5–7	27.75	–2.40
4H-2, 25–27	27.95	–2.40
4H-2, 45–47	28.15	–2.47
4H-2, 65–67	28.35	–2.32
4H-2, 85–87	28.55	–2.43
4H-2, 105–107	28.75	–2.50
4H-2, 125–127	28.95	–2.64
4H-2, 145–147	29.15	–2.66
4H-3, 5–7	29.25	–2.69
4H-3, 25–27	29.45	–2.31
4H-3, 45–47	29.65	–2.37
4H-3, 65–67	29.85	–2.61
4H-3, 85–87	30.05	–2.43
4H-3, 105–107	30.25	–2.47
4H-3, 125–127	30.45	–2.34
4H-3, 145–147	30.65	–2.48
4H-4, 5–7	30.75	–2.64
4H-4, 25–27	30.95	–2.66
4H-4, 45–47	31.15	–2.39
4H-4, 65–67	31.35	–2.37
4H-4, 85–87	31.55	–2.01
4H-4, 105–107	31.75	–2.24
4H-4, 125–127	31.95	–2.23
4H-4, 145–147	32.15	–1.75
4H-5, 5–7	32.25	–1.56
4H-5, 25–27	32.45	–1.39
4H-5, 45–47	32.65	–1.13
4H-5, 65–67	32.85	–1.13
4H-5, 85–87	33.05	–1.20
4H-5, 105–107	33.25	–1.17
4H-6, 5–7	33.75	–1.38
4H-6, 25–27	33.95	–1.38
4H-6, 45–47	34.15	–1.31
4H-6, 65–67	34.35	–1.80
4H-6, 85–87	34.55	–2.01
4H-6, 105–107	34.75	–1.78
4H-6, 125–127	34.95	–1.92
4H-6, 145–147	35.15	–1.66
4H-7, 5–7	35.25	–1.72
4H-7, 25–27	35.45	–1.71
4H-7, 44–46	35.64	–1.59
5H-1, 5–7	35.75	–1.79
5H-1, 25–27	35.95	–1.66
5H-1, 45–47	36.15	–1.66
5H-1, 65–67	36.35	–1.49
5H-1, 85–87	36.55	–1.41
5H-1, 105–107	36.75	–1.72
5H-1, 125–127	36.95	–1.57
5H-1, 141–143	37.11	–1.54
5H-2, 5–7	37.25	–1.57
5H-2, 25–27	37.45	–1.61
5H-2, 45–47	37.65	–1.67
5H-2, 65–67	37.85	–1.38
5H-2, 85–87	38.05	–1.45
5H-2, 105–107	38.25	–1.35
5H-2, 125–127	38.45	–1.49
5H-2, 141–143	38.61	–1.25
5H-3, 5–7	38.75	–1.36
5H-3, 25–27	38.95	–1.50
5H-3, 45–47	39.15	–1.48
5H-3, 65–67	39.35	–1.46
5H-3, 85–87	39.55	–1.59
5H-3, 105–107	39.75	–1.64
5H-3, 125–127	39.95	–1.58
5H-3, 141–143	40.11	–1.75
5H-4, 5–7	40.25	–1.75
5H-4, 25–27	40.45	–1.75
5H-4, 45–47	40.65	–1.76
5H-4, 65–67	40.85	–1.64
5H-4, 85–87	41.05	–1.62
5H-4, 105–107	41.25	–1.59
5H-4, 125–127	41.45	–1.55
5H-4, 141–143	41.61	–1.55
5H-5, 5–7	41.75	–1.57
5H-5, 25–27	41.95	–1.58
5H-5, 45–47	42.15	–1.59
5H-5, 65–67	42.35	–1.64
5H-5, 85–87	42.55	–1.67
5H-5, 105–107	42.75	–1.77
5H-5, 125–127	42.95	–1.59
5H-5, 141–143	43.11	–1.70
5H-6, 5–7	43.25	–1.49
5H-6, 25–27	43.45	–1.51
5H-6, 45–47	43.65	–1.62
5H-6, 65–67	43.85	–1.56
5H-6, 85–87	44.05	–1.69
5H-6, 105–107	44.25	–1.48
5H-6, 125–127	44.45	–1.64
5H-6, 141–143	44.61	–1.78
5H-7, 5–7	44.75	–1.61
5H-7, 25–27	44.95	–1.66
5H-7, 45–47	45.15	–1.69
6H-1, 5–7	45.25	–1.71
6H-1, 25–27	45.45	–1.67
6H-1, 45–47	45.65	–1.67
6H-1, 65–67	45.85	–1.98
6H-1, 85–87	46.05	–1.96
6H-1, 105–107	46.25	–1.96
6H-1, 125–127	46.45	–1.91
6H-1, 142–144	46.62	–1.98
6H-2, 5–7	46.75	–1.85
6H-2, 25–27	46.95	–1.83
6H-2, 45–47	47.15	–1.96
6H-2, 65–67	47.35	–2.15
6H-2, 85–87	47.55	–2.09
6H-2, 105–107	47.75	–2.01
6H-2, 125–127	47.95	–1.99
6H-2, 142–144	48.12	–2.04
6H-3, 5–7	48.25	–2.19
6H-3, 25–27	48.45	–2.55
6H-3, 45–47	48.65	–1.97
6H-3, 65–67	48.85	–2.01
6H-3, 85–87	49.05	–2.08
6H-3, 105–107	49.25	–1.98
6H-3, 125–127	49.45	–1.75
6H-3, 142–144	49.62	–2.18
6H-4, 5–7	49.75	–1.90
6H-4, 25–27	49.95	–1.84

Table 1 (continued).

Core, section, interval (cm)	Depth (mbsf)	$\delta^{18}O$
6H-4, 45–47	50.15	–1.96
6H-4, 65–67	50.35	–2.05
6H-4, 85–87	50.55	–2.14
6H-4, 105–107	50.75	–1.94
6H-4, 125–127	50.95	–1.93
6H-4, 142–144	51.12	–2.00
6H-5, 5–7	51.25	–2.05
6H-5, 25–27	51.45	–1.83
6H-5, 45–47	51.65	–1.44
6H-5, 65–67	51.85	–1.54
6H-5, 85–87	52.05	–1.39
6H-5, 105–107	52.25	–1.48
6H-5, 125–127	52.45	–1.46
6H-5, 142–144	52.62	–1.49
6H-6, 5–7	52.75	–1.57
6H-6, 25–27	52.95	–1.47
6H-6, 45–47	53.15	–1.39
6H-6, 65–67	53.35	–1.40
6H-6, 85–87	53.55	–1.77
6H-6, 105–107	53.75	–1.32
6H-6, 125–127	53.95	–1.33
6H-6, 142–144	54.12	–1.61
6H-7, 5–7	54.25	–1.52
6H-7, 25–27	54.45	–1.41
6H-7, 45–47	54.65	–1.55
7H-1, 5–7	54.75	–1.63
7H-1, 25–27	54.95	–1.74
7H-1, 45–47	55.15	–1.53
7H-1, 65–67	55.35	–1.53
7H-1, 85–87	55.55	–1.37
7H-1, 105–107	55.75	–1.86
7H-1, 125–127	55.95	–1.86
7H-1, 145–147	56.15	–1.45
7H-2, 5–7	56.25	–1.68
7H-2, 25–27	56.45	–1.71
7H-2, 45–47	56.65	–1.54
7H-2, 65–67	56.85	–1.52
7H-2, 85–87	57.05	–1.84
7H-2, 105–107	57.25	–1.77
7H-2, 125–127	57.45	–1.59
7H-2, 145–147	57.65	–1.41
7H-3, 5–7	57.75	–1.78
7H-3, 25–27	57.95	–1.68
7H-3, 45–47	58.15	–1.95
7H-3, 65–67	58.35	–1.54
7H-3, 85–87	58.55	–1.50
7H-3, 105–107	58.75	–1.71
7H-3, 125–127	58.95	–1.69
7H-3, 145–147	59.15	–2.05
7H-4, 5–7	59.25	–1.99
7H-4, 25–27	59.45	–1.89
7H-4, 45–47	59.65	–1.83
7H-4, 65–67	59.85	–1.98
7H-4, 85–87	60.05	–1.63
7H-4, 105–107	60.25	–1.77
7H-4, 125–127	60.45	–2.22
7H-4, 145–147	60.65	–2.06
7H-5, 5–7	60.75	–1.96
7H-5, 25–27	60.95	–2.05
7H-5, 45–47	61.15	–2.08
7H-5, 65–67	61.35	–2.04
7H-5, 85–87	61.55	–1.77
7H-5, 105–107	61.75	–2.18
7H-6, 5–7	62.25	–2.08
7H-6, 25–27	62.45	–2.01
7H-6, 45–47	62.65	–1.98
7H-6, 65–67	62.85	–2.07
7H-6, 85–87	63.05	–2.17
7H-6, 105–107	63.25	–1.95
7H-6, 125–127	63.45	–2.02
7H-7, 5–7	63.75	–2.00
8H-1, 5–7	64.25	–1.52
8H-1, 25–27	64.45	–1.17
8H-1, 45–47	64.65	–1.21
8H-1, 65–67	64.85	–1.11
8H-1, 85–87	65.05	–1.16
8H-1, 105–107	65.25	–1.11
8H-1, 125–127	65.45	–1.28
8H-1, 145–147	65.65	–1.22
8H-2, 5–7	65.75	–1.28
8H-2, 25–27	65.95	–1.26
8H-2, 45–47	66.15	–1.26
8H-2, 65–67	66.35	–1.26
8H-2, 85–87	66.55	–1.27
8H-2, 105–107	66.75	–1.13
8H-2, 125–127	66.95	–1.23
8H-2, 145–147	67.15	–1.36
8H-3, 5–7	67.25	–1.33
8H-3, 25–27	67.45	–1.25
8H-3, 45–47	67.65	–1.29
8H-3, 65–67	67.85	–1.30
8H-3, 85–87	68.05	–1.30
8H-3, 105–107	68.25	–1.21
8H-3, 125–127	68.45	–1.03
8H-3, 145–147	68.65	–0.96
8H-4, 5–7	68.75	–1.00
8H-4, 25–27	68.95	–1.04
8H-4, 45–47	69.15	–0.86
8H-4, 65–67	69.35	–0.78
8H-4, 85–87	69.55	–1.13
8H-4, 105–107	69.75	–0.81
8H-4, 125–127	69.95	–1.01
8H-4, 145–147	70.15	–0.99
8H-5, 5–7	70.25	–1.24
8H-5, 25–27	70.45	–0.92
8H-5, 45–47	70.65	–1.31
8H-5, 65–67	70.85	–1.31
8H-5, 85–87	71.05	–1.61
8H-5, 105–107	71.25	–1.33
8H-5, 125–127	71.45	–1.59
8H-6, 5–7	71.75	–1.66
8H-6, 25–27	71.95	–1.83
8H-6, 45–47	72.15	–1.83
8H-6, 65–67	72.35	–1.78
8H-6, 85–87	72.55	–1.66
8H-6, 105–107	72.75	–1.69
8H-6, 125–127	72.95	–1.76
8H-6, 145–147	73.15	–1.72
8H-7, 5–7	73.25	–1.66
8H-7, 25–27	73.45	–1.67
8H-7, 45–47	73.65	–1.57
8H-7, 65–67	73.85	–1.57
9H-1, 5–7	73.75	–1.51
9H-1, 25–27	73.95	–1.42
9H-1, 45–47	74.15	–1.51
9H-1, 65–67	74.35	–1.34
9H-1, 85–87	74.55	–1.50
9H-1, 105–107	74.75	–1.51
9H-1, 125–127	74.95	–1.37
9H-1, 145–147	75.15	–1.31
9H-2, 5–7	75.25	–1.39
9H-2, 25–27	75.45	–1.22
9H-2, 45–47	75.65	–1.23
9H-2, 65–67	75.85	–1.56
9H-2, 85–87	76.05	–1.51
9H-2, 105–107	76.25	–1.45
9H-2, 125–127	76.45	–1.66
9H-2, 145–147	76.65	–1.53
9H-3, 5–7	76.75	–1.55
9H-3, 25–27	76.95	–1.93
9H-3, 45–47	77.15	–1.53
9H-3, 65–67	77.35	–1.74
9H-3, 85–87	77.55	–1.70
9H-3, 105–107	77.75	–1.72
9H-3, 125–127	77.95	–1.77
9H-3, 145–147	78.15	–1.39
9H-4, 5–7	78.25	–1.21
9H-4, 25–27	78.45	–1.38
9H-4, 45–47	78.65	–1.51
9H-4, 65–67	78.85	–1.51
9H-4, 85–87	79.05	–1.03
9H-4, 105–107	79.25	–0.96
9H-4, 125–127	79.45	–0.68
9H-5, 5–7	79.75	–0.68
9H-5, 25–27	79.95	–0.55
9H-5, 45–47	80.15	–0.95
9H-5, 65–67	80.35	–0.84
9H-5, 85–87	80.55	–1.03
9H-5, 105–107	80.75	–1.05
9H-5, 125–127	80.95	–1.22
9H-6, 5–7	81.25	–1.24
9H-6, 25–27	81.45	–1.29
9H-6, 45–47	81.65	–1.33
9H-6, 65–67	81.85	–1.72
9H-6, 85–87	82.05	–1.71
9H-6, 105–107	82.25	–1.76
9H-6, 125–127	82.45	–1.63
9H-6, 145–147	82.65	–1.49
9H-7, 5–7	82.75	–1.42
9H-7, 25–27	82.95	–1.09
9H-7, 45–47	83.15	–0.99
10H-1, 5–7	83.25	–0.88
10H-1, 24–26	83.44	–0.94
10H-1, 44–46	83.64	–0.81
10H-1, 64–66	83.84	–0.86
10H-1, 85–87	84.05	–0.63
10H-1, 105–10	84.25	–0.54
10H-1, 125–12	84.45	–0.71
10H-1, 145–14	84.65	–0.30
10H-2, 5–7	84.75	–0.38
10H-2, 24–26	84.94	–0.08
10H-2, 44–46	85.14	–0.55
10H-2, 64–66	85.34	–0.56
10H-2, 85–87	85.55	–0.64
10H-2, 105–10	85.75	–0.54
10H-2, 125–12	85.95	–0.40
10H-2, 145–14	86.15	–0.28
10H-3, 5–7	86.25	–0.38
10H-3, 24–26	86.44	–0.43
10H-3, 44–46	86.64	–0.33
10H-3, 64–66	86.84	–0.47
10H-3, 85–87	87.05	–0.35
10H-3, 105–10	87.25	–0.40
10H-3, 125–12	87.45	–0.45
10H-3, 145–14	87.65	–0.50
10H-4, 5–7	87.75	–0.48
10H-4, 24–26	87.94	–0.69
10H-4, 44–46	88.14	–0.84
10H-4, 64–66	88.34	–1.17
10H-4, 85–87	88.55	–1.59
10H-4, 105–10	88.75	–1.74
10H-4, 125–12	88.95	–1.70
10H-4, 145–14	89.15	–1.85
10H-5, 5–7	89.25	–1.47
10H-5, 24–26	89.44	–0.99
10H-5, 44–46	89.64	–0.69
10H-5, 64–66	89.84	–0.91
10H-5, 85–87	90.05	–0.78
10H-5, 105–10	90.25	–0.83
10H-5, 125–12	90.45	–1.11
10H-6, 5–7	90.75	–0.92
10H-6, 24–26	90.94	–1.14
10H-6, 44–46	91.14	–0.96
10H-6, 64–66	91.34	–0.82
10H-6, 85–87	91.55	–1.08
10H-6, 105–10	91.75	–0.98
10H-6, 125–12	91.95	–1.42
10H-6, 145–14	92.15	–1.16
10H-7, 5–7	92.25	–1.22
10H-7, 24–26	92.44	–1.26
10H-7, 44–46	92.64	–1.33
10H-7, 64–66	92.84	–1.37
11H-1, 5–7	92.75	–1.13
11H-1, 24–26	92.94	–1.42
11H-1, 44–46	93.14	–1.47
11H-1, 64–66	93.34	–1.34
11H-1, 84–86	93.54	–1.32
11H-1, 104–10	93.74	–1.42
11H-1, 124–12	93.94	–1.30
11H-1, 144–14	94.14	–1.51
11H-2, 5–7	94.25	–1.01
11H-2, 24–26	94.44	–0.89
11H-2, 44–46	94.64	–0.83
11H-2, 64–66	94.84	–0.87
11H-2, 84–86	95.04	–0.78
11H-2, 104–10	95.24	–0.83
11H-2, 124–12	95.44	–0.89
11H-2, 144–14	95.64	–0.46
11H-3, 5–7	95.75	–0.51
11H-3, 24–26	95.94	–0.70
11H-3, 44–46	96.14	–0.72
11H-3, 64–66	96.34	–0.69
11H-3, 84–86	96.54	–0.67
11H-3, 104–10	96.74	–0.78
11H-3, 124–12	96.94	–0.73
11H-3, 144–14	97.14	–0.77
11H-4, 5–7	97.25	–0.77
11H-4, 24–26	97.44	–0.67
11H-4, 44–46	97.64	–0.86
11H-4, 64–66	97.84	–0.76
11H-4, 84–86	98.04	–0.78
11H-4, 104–10	98.24	–0.86
11H-4, 124–12	98.44	–0.90
11H-4, 144–14	98.64	–0.75
11H-5, 5–7	98.75	–0.82
11H-5, 24–26	98.94	–0.65
11H-5, 44–46	99.14	–1.05
11H-5, 64–66	99.34	–0.74
11H-5, 84–86	99.54	–0.89
11H-5, 104–10	99.74	–0.92
11H-5, 124–12	99.94	–0.96
11H-5, 144–14	100.14	–0.86
11H-6, 5–7	100.25	–0.85
11H-6, 24–26	100.44	–0.71
11H-6, 44–46	100.64	–1.00
11H-6, 64–66	100.84	–1.07
11H-6, 84–86	101.04	–0.69

Table 1 (continued).

Core, section, interval (cm)	Depth (mbsf)	$\delta^{18}O$
11H-6, 104–10	101.24	–0.55
11H-6, 124–12	101.44	–0.66
11H-6, 144–14	101.64	–0.65
11H-7, 5–7	101.75	–0.58
12H-1, 5–7	102.25	–0.41
12H-1, 24–26	102.44	–0.69
12H-1, 44–46	102.64	–0.32
12H-1, 64–66	102.84	–0.30
12H-1, 84–86	103.04	–0.56
12H-1, 104–10	103.24	–0.57
12H-1, 124–12	103.44	–0.59
12H-1, 144–14	103.64	–0.67
12H-2, 5–7	103.75	–0.73
12H-2, 24–26	103.94	–0.79
12H-2, 44–46	104.14	–1.52
12H-2, 64–66	104.34	–1.72
12H-2, 84–86	104.54	–0.99
12H-2, 104–10	104.74	–1.01
12H-2, 124–12	104.94	–0.56
12H-2, 144–14	105.14	–0.60
12H-3, 5–7	105.25	–0.64
12H-3, 24–26	105.44	–0.77
12H-3, 44–46	105.64	–0.68
12H-3, 64–66	105.84	–0.64
12H-3, 84–86	106.04	–0.95
12H-3, 104–10	106.24	–1.27
12H-3, 124–12	106.44	–1.28
12H-3, 144–14	106.64	–0.80
12H-4, 5–7	106.75	–1.13
12H-4, 24–26	106.94	–0.83
12H-4, 44–46	107.14	–0.62
12H-4, 64–66	107.34	–0.41
12H-4, 84–86	107.54	–0.17
12H-4, 104–10	107.74	–0.12
12H-4, 124–12	107.94	–0.24
12H-4, 144–14	108.14	+0.09
12H-5, 5–7	108.25	–0.37
12H-5, 24–26	108.44	–0.13
12H-5, 44–46	108.64	–0.26
12H-5, 64–66	108.84	–0.37
12H-5, 84–86	109.04	–0.23
12H-5, 104–10	109.24	–0.25
12H-5, 124–12	109.44	–0.20
12H-5, 144–14	109.64	–0.29
12H-6, 5–7	109.75	–0.34
12H-6, 24–26	109.94	–0.36
12H-6, 44–46	110.14	–0.54
12H-6, 64–66	110.34	–0.57
12H-6, 84–86	110.54	–0.61
12H-6, 104–10	110.74	–0.67
12H-6, 124–12	110.94	–0.62
12H-6, 144–14	111.14	–0.58
12H-7, 5–7	111.25	–0.91
12H-7, 24–26	111.44	–0.64
12H-7, 44–46	111.64	–0.66
12H-7, 64–66	111.84	–0.59
13H-1, 5–7	111.75	–0.86
13H-1, 25–27	111.95	–0.77
13H-1, 45–47	112.15	–0.57
13H-1, 65–67	112.35	–0.48
13H-1, 85–87	112.55	–0.47
13H-1, 105–10	112.75	–0.72
13H-1, 125–12	112.95	–0.90
13H-1, 145–14	113.15	–0.29
13H-2, 5–7	113.25	–0.40
13H-2, 25–27	113.45	–0.56
13H-2, 45–47	113.65	–0.54
13H-2, 65–67	113.85	–0.43
13H-2, 85–87	114.05	–0.32
13H-2, 105–10	114.25	–0.29
13H-2, 125–12	114.45	–0.44
13H-2, 145–14	114.65	–0.10
13H-3, 5–7	114.75	–0.31
13H-3, 25–27	114.95	–0.32
13H-3, 45–47	115.15	–0.30
13H-3, 65–67	115.35	–0.30
13H-3, 85–87	115.55	–0.39
13H-3, 105–10	115.75	–0.35
13H-3, 125–12	115.95	–0.74
13H-3, 145–14	116.15	–0.65
13H-4, 5–7	116.25	–0.64
13H-4, 25–27	116.45	–0.71
13H-4, 45–47	116.65	–0.80
13H-4, 65–67	116.85	–0.81
13H-4, 85–87	117.05	–1.22
13H-4, 105–10	117.25	–1.32
13H-4, 125–12	117.45	–1.45
13H-5, 5–7	117.75	–1.54
13H-5, 25–27	117.95	–1.61
13H-5, 45–47	118.15	–1.69
13H-5, 65–67	118.35	–1.84
13H-5, 85–87	118.55	–1.91
13H-5, 105–10	118.75	–1.74
13H-5, 125–12	118.95	–1.67
13H-6, 5–7	119.25	–1.34
13H-6, 25–27	119.45	–0.94
13H-6, 45–47	119.65	–0.70
13H-6, 65–67	119.85	–0.61
13H-6, 85–87	120.05	–0.28
13H-6, 105–10	120.25	–0.46
13H-6, 125–12	120.45	–0.70
13H-6, 145–14	120.65	–0.81
13H-7, 5–7	120.75	–0.78
13H-7, 25–27	120.95	–0.59
13H-7, 45–47	121.15	–0.41
14H-1, 5–7	121.25	–0.45
14H-1, 25–27	121.45	–0.56
14H-1, 45–47	121.65	–0.66
14H-1, 65–67	121.85	–0.73
14H-1, 85–87	122.05	–0.79
14H-1, 105–10	122.25	–0.86
14H-1, 125–12	122.45	–1.17
14H-1, 145–14	122.65	–1.25
14H-2, 5–7	122.75	–1.34
14H-2, 24–26	122.94	–0.92
14H-2, 45–47	123.15	–0.39
14H-2, 65–67	123.35	–0.78
14H-2, 82–84	123.52	–0.59
14H-3, 5–7	123.80	–0.72
14H-3, 24–26	123.99	–0.74
14H-3, 48–50	124.23	–0.17
14H-3, 65–67	124.40	–0.10
14H-3, 82–84	124.57	–0.63
14H-3, 106–10	124.81	–1.58
14H-3, 125–12	125.00	–1.76
14H-3, 145–14	125.20	–1.48
14H-4, 5–7	125.32	–1.72
14H-4, 28–30	125.55	–1.60
14H-4, 45–47	125.72	–1.51
14H-4, 64–66	125.91	–1.11
14H-5, 28–30	126.23	–1.39
14H-5, 45–47	126.40	–1.24
14H-5, 64–66	126.59	–1.16
14H-5, 85–87	126.80	–1.16
14H-5, 106–10	127.01	–1.31
14H-5, 122–12	127.17	–0.67
14H-5, 145–14	127.40	–0.93
14H-6, 5–7	127.50	–1.15
14H-6, 25–27	127.70	–1.15
14H-6, 45–47	127.90	–1.15
14H-6, 65–67	128.10	–0.98
14H-6, 79–81	128.24	–1.10
14H-7, 5–7	128.30	–0.93
14H-7, 25–27	128.50	–0.77
14H-7, 47–49	128.72	–1.06
14H-7, 66–68	128.91	–0.35
14H-7, 85–87	129.10	–0.46
14H-7, 105–10	129.30	–0.47
14H-7, 125–12	129.50	–0.49
14H-7, 145–14	129.70	–0.77
14H-8, 5–7	129.80	–0.71
14H-8, 25–27	130.00	–0.85
14H-CC, 5–7	130.10	–1.47
14H-CC, 18–20	130.23	–1.46
15H-1, 5–7	130.75	–0.95
15H-1, 25–27	130.95	–0.84
15H-1, 45–47	131.15	–0.86
15H-1, 65–67	131.35	–0.79
15H-1, 85–87	131.55	–1.54
15H-1, 105–10	131.75	–1.61
15H-1, 125–12	131.95	–1.28
15H-1, 145–14	132.15	–1.42
15H-2, 5–7	132.25	–0.77
15H-2, 25–27	132.45	–0.42
15H-2, 45–47	132.65	–0.35
15H-2, 65–67	132.85	–0.19
15H-2, 85–87	133.05	+0.10
15H-2, 105–10	133.25	+0.09
15H-2, 125–12	133.45	–0.15
15H-2, 145–14	133.65	–0.01
15H-3, 5–7	133.75	+0.03
15H-3, 25–27	133.95	+0.05
15H-3, 45–47	134.15	+0.08
15H-3, 65–67	134.35	+0.11

Core, section, interval (cm)	Depth (mbsf)	Adj. dbsf	$\delta^{18}O$
133- 820B-			
15H-1, 25-27	131.95	134.15	-0.14
15H-1, 45-47	132.15	134.35	0.07
15H-1, 65-67	132.35	134.55	0.13
15H-1, 85-87	132.55	134.75	0.14
15H-1, 105-107	132.75	134.95	0.12
15H-1, 122-124	132.92	135.12	-0.08
15H-1, 145-147	133.15	135.35	0.10
15H-2, 5-7	133.25	135.45	0.29
15H-2, 25-27	133.45	135.65	0.16
15H-2, 45-47	133.65	135.85	0.02
15H-2, 65-67	133.85	136.05	-0.12
15H-2, 85-87	134.05	136.25	0.03
15H-2, 105-107	134.25	136.45	-0.19
15H-2, 122-124	134.42	136.62	-0.43
15H-2, 145-147	134.65	136.85	-0.55
15H-3, 5-7	134.75	136.95	-0.37
15H-3, 25-27	134.95	137.15	-0.20
15H-3, 45-47	135.15	137.35	-0.98
15H-3, 65-67	135.35	137.55	-1.05
15H-3, 85-87	135.55	137.75	-1.06
15H-3, 145-147	136.15	138.35	-1.12
15H-4, 5-7	136.25	138.45	-1.25
15H-4, 25-27	136.45	138.65	-1.30
15H-4, 45-47	136.65	138.85	-1.25
15H-4, 65-67	136.85	139.05	-0.90
15H-4, 85-87	137.05	139.25	-0.74
15H-4, 105-107	137.25	139.45	-0.92
15H-4, 122-124	137.42	139.62	-0.90
15H-4, 145-147	137.65	139.85	-0.97
15H-5, 5-7	137.75	139.95	-0.86
15H-5, 25-27	137.95	140.15	0.11
15H-5, 45-47	138.15	140.35	-0.42
15H-5, 65-67	138.35	140.55	-0.15
15H-5, 85-87	138.55	140.75	-0.51
15H-5, 105-107	138.75	140.95	-0.13
15H-5, 122-124	138.92	141.12	0.04
15H-5, 145-147	139.15	141.35	-0.09
15H-6, 5-7	139.25	141.45	-0.10
15H-6, 25-27	139.45	141.65	-0.62
15H-6, 45-47	139.65	141.85	-0.37
15H-6, 65-67	139.85	142.05	-0.12
15H-6, 85-87	140.05	142.25	-0.11
15H-6, 105-107	140.25	142.45	-0.87
15H-6, 122-124	140.42	142.62	-0.24
15H-6, 145-147	140.65	142.85	-0.59
15H-7, 5-7	140.75	142.95	-0.51
15H-7, 25-27	140.95	143.15	-0.62
15H-7, 45-47	141.15	143.35	-0.74
15H-7, 65-67	141.25	143.45	-0.46
16H-1, 24-26	141.44	143.64	-0.83
16H-1, 44-46	141.64	143.84	-1.90
16H-1, 64-66	141.84	144.04	-1.12
16H-1, 83-85	142.03	144.23	-0.52
16H-1, 105-107	142.25	144.45	-1.30
16H-1, 145-147	142.65	144.85	-1.94
16H-2, 5-7	142.75	144.95	-1.82
16H-2, 25-27	142.95	145.15	-1.68
16H-2, 44-46	143.14	145.34	-1.72
16H-2, 64-66	143.34	145.54	-1.77
16H-2, 85-87	143.55	145.75	-1.69
16H-2, 105-107	143.75	145.95	-0.72
16H-2, 120-122	143.90	146.10	-0.85
16H-2, 145-147	144.15	146.35	-1.56
16H-3, 6-8	144.26	146.46	-1.36
16H-3, 50-52	144.70	146.90	-1.34
16H-4, 58-60	146.28	148.48	-0.46
16H-4, 125-127	146.95	149.15	-0.79
16H-5, 145-147	148.65	150.85	-0.82
16H-CC, 8-10	148.78	150.98	-1.08
17H-1, 25-27	150.95	153.15	-1.04

Table 2. Duplicate $\delta^{18}O$ measurements of separate aliquots of *G. ruber* from the upper 10 m of Hole 820A.

Core, section, interval (cm)	Depth (mbsf)	$\delta^{18}O$ (‰)	$\delta^{18}O$ (‰)	$\Delta\delta^{18}O$ (‰)
133-820A-				
1H-1, 5–7	0.05	–2.270	–2.280	0.010
1H-1, 25–27	0.25	–2.287	–2.264	0.023
1H-1, 45–47	0.45	–2.384	–2.315	0.069
1H-1, 85–87	0.85	–2.477	–2.308	0.169
1H-1, 105–107	1.05	–2.365	–2.646	0.281
1H-1, 125–127	1.25	–2.321	–2.179	0.142
1H-1, 145–147	1.45	–2.084	–2.149	0.065
1H-2, 5–7	1.55	–2.076	–2.327	0.251
1H-2, 25–27	1.75	–2.512	–2.561	0.049
1H-2, 45–47	1.95	–2.593	–2.597	0.004
1H-2, 65–67	2.15	–2.639	–2.371	0.268
1H-2, 85–87	2.35	–2.643	–2.458	0.185
1H-2, 105–107	2.55	–2.628	–2.518	0.110
1H-2, 125–127	2.75	–2.401	–2.578	0.177
1H-2, 145–147	2.95	–2.2526	–2.509	0.017
1H-3, 5–7	3.05	–2.536	–2.404	0.132
1H-3, 25–27	3.25	–2.519	–2.645	0.126
1H-3, 45–47	3.45	–2.271	–2.655	0.384
1H-3, 65–67	3.65	–2.179	–2.158	0.021
1H-3, 85–87	3.85	–2.183	–2.327	0.144
1H-3, 105–107	4.05	–2.407	–2.531	0.124
1H-3, 145–147	4.45	–1.935	–2.111	0.176
1H-4, 45–47	4.95	–2.167	–2.209	0.042
1H-4, 65–67	5.15	–2.202	–2.428	0.226
1H-4, 125–127	5.75	–2.134	–2.050	0.084
1H-5, 5–7	6.05	–2.215	–2.380	0.165
1H-5, 25–27	6.25	–1.772	–2.007	0.235
1H-5, 45–47	6.45	–1.813	–2.035	0.222
1H-5, 65–67	6.65	–1.815	–1.917	0.102
1H-5, 85–87	6.85	–1.615	–1.668	0.053
1H-5, 93–98	6.93	–1.681	–1.516	0.165
2H-1, 5–7	7.25	–0.975	–1.251	0.276
2H-1, 25–27	7.45	–1.368	–1.285	0.083
2H-1, 45–47	7.65	–1.442	–1.403	0.039
2H-1, 65–67	7.85	–1.609	–1.512	0.097
2H-1, 85–87	8.05	–1.862	–1.799	0.063
2H-1, 105–107	8.25	–1.779	–1.542	0.237
2H-1, 125–127	8.45	–1.738	–1.876	0.138
2H-2, 5–7	8.75	–1.779	–1.900	0.121
2H-2, 25–27	8.95	–1.691	–1.793	0.102

Note: Column 5 ($\Delta\delta^{18}O$) lists the difference (‰) between duplicate measurements.

magnetic data although most compatible with the deeper end of the proposed range.

Above 80 mbsf, however, the age-structure outlined above does not agree with the nannostratigraphy for Hole 820A that proposes nannofossil ages of 275 k.y. (lowest occurrence [LO] of *Emiliania huxleyi*) at 35.8 mbsf and 75 k.y. (LO of *Emiliania huxleyi* Acme) at 12.1 mbsf in Hole 820A (Wei and Gartner, in press). According to these ages, the first interpretation of the age-structure (based on pattern-matching) is not correct, because (1) stage 6 (128–186 k.y.: Imbrie et al., 1984), found between 31.55 and 39.35 mbsf, cannot be dated at 275 k.y., and (2) stage 4 and event 3.3 (58.96–73.91 and 55.45 k.y., respectively; Martinson et al., 1987), found between 7 and 22.63 mbsf, cannot be dated as 75,000 yr. Therefore, a second age model for the upper 80 m in Hole 820A is proposed. This age model is presented in Figure 4B. To refine the paleodating of the first section further, the first appearance of the planktonic foraminifer *Bolliela calida calida* is determined, found at a depth of 38.45 to 40.11 mbsf in Hole 820A (Chaproniere, pers. comm., 1991) and dated as 140,000 yr (Bolli and Premoli Silva, 1973). This datum, therefore, does not comply with the 275,000-yr datum, as it lies stratigraphically lower and is thought to be younger than the *Emiliania huxleyi* datum. The first appearance of *Bolliela calida calida,* however, appears to follow the first age-structure.

Nevertheless, the results of the second age model, which are shown in Figure 4B, indicate that all stages except stages 4 and 7 are present. Both stages 3 and 6 appear incomplete. Two hiatuses therefore occur: the first hiatus, between 34.55 and 35.8 mbsf (event 6.5), spans at least the time interval for stage 7 between 186 and 245 k.y.

Table 3. Boundaries of the interpreted oxygen-isotope stages for Holes 820A and 820B and their corresponding depths below seafloor.

Stage boundary	Depth (mbsf)
1–2	6.45
2–3	7.78
3–4	21.45
4–5	23.55
5–6	32.10
(6–7	45.85)
(7–8	64.25)
8–9	77.65
9–10	83.64
10–11	88.34
11–12	94.84
12–13	103.75
13–14	106.44
14–15	117.05
15–16	132.25
16–17	136.95
17–18	139.85
18–19	144.45

Note: Boundaries and depths bounded by parentheses apply to the first age model discussed in text.

(Imbrie et al., 1984). As a consequence, stage 8 stretches from 76.05 to 35.8 mbsf, with the high $\delta^{18}O$ values at 42, 52, and 67 mbsf interpreted as isotopic events 8.2, 8.4, and 8.6, respectively (Prell et al., 1986). The second hiatus spans at least the time interval for stage 4 from 58 to 74 k.y. between 8.05 (event 3.1) and 12.1 mbsf. Consequently, stage 5 expands from 29.25 to 12.1.

In the following discussion, we will use the second age model for determining time-frequency spectra, because this model is more compatible with the biostratigraphic calcareous nannofossil ages for Hole 820A, commonly used in globally related isotope studies and throughout this volume.

DISCUSSION

The maximum $\delta^{18}O$ values of stage 16 in Holes 820A and 820B (Fig. 3) are similar to those in stage 10 (~+0.1‰ vs. PDB). This agrees with results from Hole 677A, where oxygen-isotope stage 10 is of similar magnitude to the most extensive glacials of the Brunhes Chron (Shackleton and Hall, 1989). However, in comparison to stages 6 and 2, isotope stage 16 in Hole 820A has $\delta^{18}O$ values 1.0‰ greater than those in Hole 677A , where the $\delta^{18}O$ values of stages 2, 6, 16, and 22 vary only within 0.3‰. In this regard, the $\delta^{18}O$ values for Hole 819A (Kroon et al., this volume) are similar to those from Hole 820A, and most likely indicate a regional influence, possibly associated with a progressive increase in temperature throughout the late Pleistocene.

In an attempt to extract this regional variation, we calculated the difference of the isotope signal of Hole 820A from that in Hole 677A for successive equivalent glacial and interglacial stages for both of the age interpretations outlined above. These calculations are summarized in Table 4 and represent the deviation of the $\delta^{18}O$ values from Holes 820A and 820B from those in Hole 677A, normalized to isotope stage 2 of Hole 820A.

The results are represented by the black dots in Figure 5. The black dots bounded by parentheses were calculated on the basis of proposed isotopic events 7.0, 7.5, 8.4, 8.5, and 8.6 in the first interpretation. Clearly, the deviations of the glacial/interglacial $\delta^{18}O$ values between both holes become less (approximately 1‰) over the last 19 stages. Deviations for stages 10 to 19 vary from +1.21‰ at stage 11 to +0.60‰ at stage 10, with increased deviations occurring at glacial and smaller deviations at interglacial stages. If these differences were ascribed to sea-surface temperature variations alone, this would imply fluctuations in temperatures of up to 2.0°C, with regionally higher temperatures at Site 820 during interglacial periods.

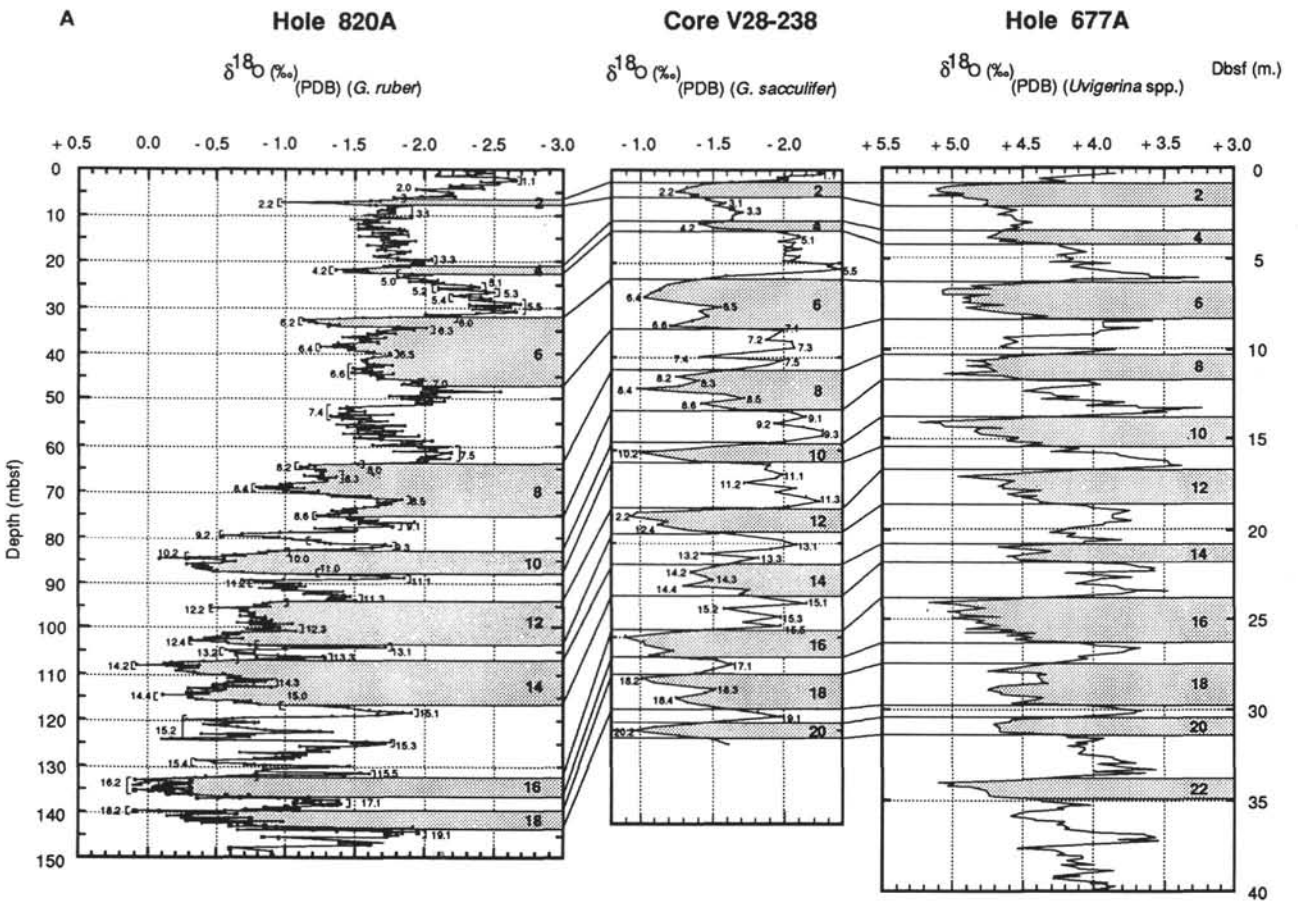

Figure 4. **A.** Age model 1—Oxygen-isotope stratigraphy for Holes 820A and 820B, interpreted through correlation with Core V28-238 (Shackleton and Opdyke, 1973) and Hole 677A (Shackleton and Hall, 1989), using the graphic correlation concept outlined by Prell et al. (1986). **B.** Age model 2—Oxygen-isotope stratigraphy of Holes 820A and 820B in comparison to the isotope chronostratigraphy of Hole 607A (Ruddiman et al., 1989) and 677A (Shackleton, et al., 1990). The paleontological ages (75, 275, 465 k.y.) in Hole 820A are based on calcareous nannofossil stratigraphy determined by Wei and Gartner (this volume). In addition, the ages of 120,000 and 140,000 yr were determined by shore-based studies on the basis of the last appearance of *Globigerinoides ruber* pink and first appearance of *Bolliela calida calida,* respectively (Chaproniere, pers. comm., 1991). The 730,000 yr datum is based on the position of the Brunhes/Matuyama reversal boundary, proposed by Barton et al. (this volume).

Furthermore, the transition from stages 10 to 9, for both age interpretations, is marked by a progressive decrease in deviation of $\delta^{18}O$ between the two holes from stage 10, through stage 9 to the early part of stage 8. This change in deviation, from +0.77 to –0.43‰, suggests a possible increase of 4°C in sea-surface temperature.

Finally, deviations between Holes 820A and 667A for glacial and interglacial values of stages 6 to 1 suggest coherent $\delta^{18}O$ values of approximately –0.1‰ for the upper part of Hole 820A. An exception is stage 3, which displays a deviation that is approximately 0.25‰ lower than the $\delta^{18}O$ value of isotope stage 3 in Hole 677A.

The proposed increase of 4°C in sea-surface temperature at Site 820, which occurs from approximately 400 k.y. (~80 mbsf) coincides with changes in seismic character (Feary et al., this volume), lithologies (Feary and Jarrard, this volume; Barton et al., this volume), log characteristics (Davies et al., 1991), and geochemical variables (Feary and Jarrard, this volume) at Site 820.

Also, coincident with the proposed increase in surface temperature we observe a change in the frequency of the $\delta^{18}O$ signal in Hole 820A. To investigate these observations further, we established time-frequency spectra for the $\delta^{18}O$ record for the two identified intervals (Fig. 6). In the time interval from 0 to 400 k.y. (stages 1 to 10; Imbrie et al., 1984), the dominant power occurs at 135 k.y. with little power at higher frequencies. Between 400 and 730 k.y. (B/M boundary or stage 19.1), the power is most significant at 45 and 37 k.y., with 45 k.y. slightly dominant over the 37 k.y. frequency. Clearly, differences exist for the intervals above and below the boundary having an age of approximately 400 k.y. younger than which, the 135 k.y. frequency dominates almost totally, and older than which, frequencies of 45 and 37 k.y. dominate. These are apparently not the Milankovitch periodicities that are normally observed in deep-sea sediments (Imbrie et al., 1984). However, their divergence from the Milankovitch cycles may be the result of variations in sedimentation rates and the relatively poor time control for such a high-resolution section. Nevertheless, the obtained spectra support a major difference in the cyclic behavior of the isotope signal of Hole 820A for intervals younger and older than 400 k.y.

Changes in the frequency of isotopic variation of middle and late Pleistocene sections have been noted by other researchers and interpreted in one of two ways: (1) Prell (1982) and Maasch (1988) proposed a rapid change in frequency at about 900,000 yr; (2) Imbrie (1985) and Ruddiman (1986, 1989) favored a gradual change in frequency between 780 and 400 k.y., with an acceleration between 700 and 600 k.y. Our data (indicating a marked change in frequency for intervals younger and older than 400,000 yr) thus accord in general with both the above interpretations. Furthermore, we postulate that the frequency change was accompanied by a progressive temperature increase over a maximum time interval between 400 and 275,000 yr.

We are unclear as to how the frequency variation in the isotope signal, possible temperature change, and changes in sediment patterns

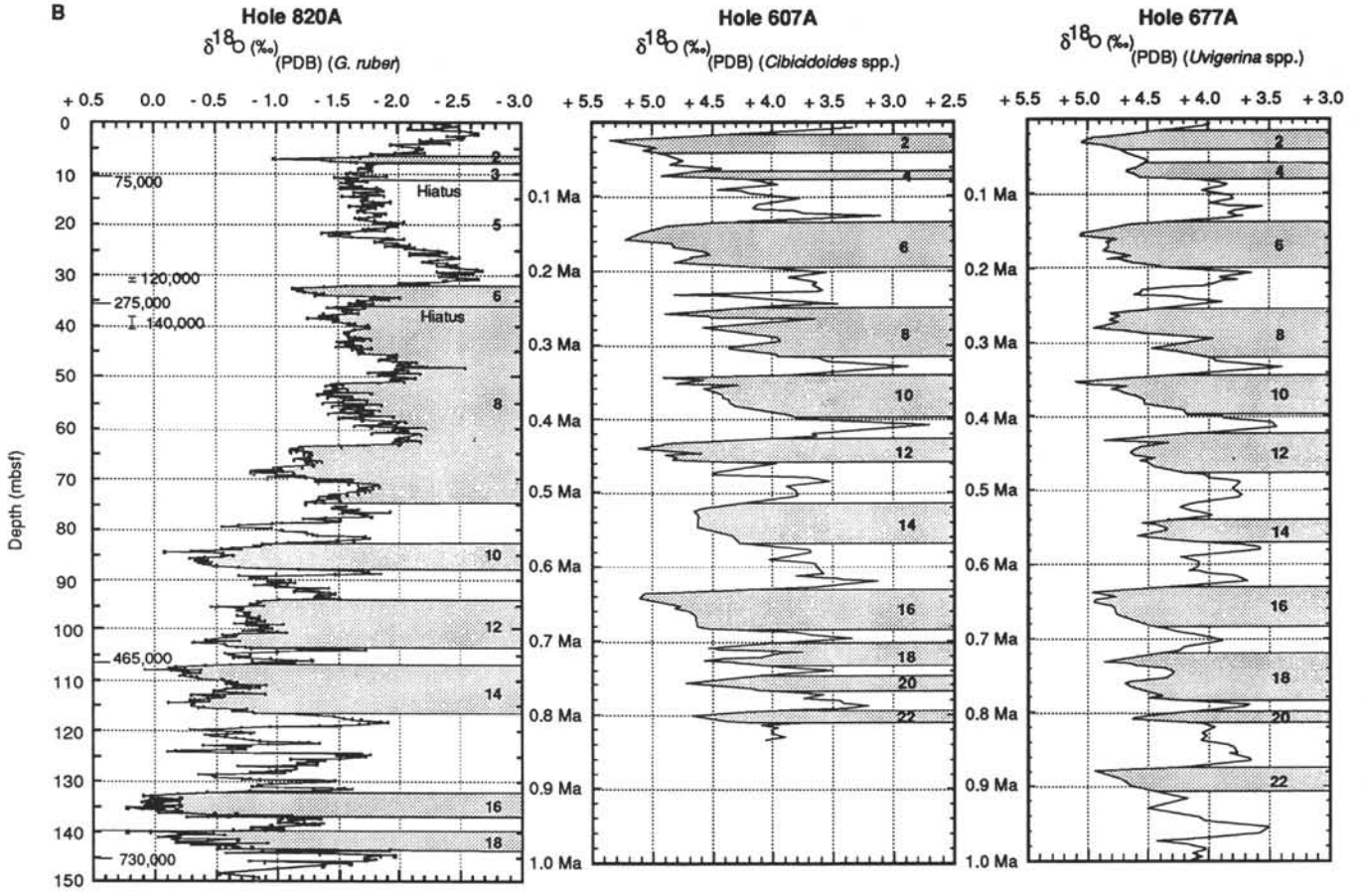

Figure 4 (continued).

are related. However, the fact that they appear seems beyond coincidence. Therefore, we suggest that a climatic or regional factor raised sea-surface temperatures over northeastern Australia about 400 k.y. ago, which in turn catalyzed the growth of the Great Barrier Reef. Such a system would then have had a profound effect on sediment patterns and geometries thereafter.

Despite these suggestions, we cannot exclude the possible effects of diagenesis on the obtained $\delta^{18}O$ signal. Although foraminifers have been cleaned and chosen carefully, diagenetic alterations, may have occurred. Feary and Jarrard (this volume) report on the development of cemented aggregates, particularly between 100 and 150 mbsf, while Davies and others (1991) described a downward increase in Sr^{2+} content and decrease in Mg^{2+} and Ca^{2+} contents in the pore waters in the upper 100 m of Site 820, probably associated with the formation of authigenic calcite and dolomite. However, considering (1) the coherence of the isotope signal of Holes 820A and 820B; (2) the same isotopic shift seen in Hole 819A at approximately the same time (Kroon et al., this volume); and (3) the occurrence of cemented aggregates, mostly below 100 mbsf, we think that diagenesis is less important than the climate signal in the isotope record of Hole 820A and that it does not affect our findings and conclusions. Trace-element studies in progress (Ca, Mg, and Sr) on the foraminifers themselves may increase our knowledge about the subject of diagenesis at Site 820.

CONCLUSIONS

A coherent, high-resolution, oxygen-isotope signal has been established from planktonic foraminifers for the upper 145 m of Site 820 in 280 m of water off the northeastern Australian margin.

Isotope stages 1 to 19 have been interpreted on the basis of pattern-matching with other deep-sea cores and have been guided by the paleontological datums from Hole 820A that were established during drilling. On these bases, we think that isotope stages 4 and 7 are missing and are represented by two hiatuses at depths of 8.02 to 12.1 and 34.55 and 35.8 mbsf.

Using isotope data from Hole 677A as a reference curve, a regional isotopic change for the northeastern Australian margin has been calculated that, if interpreted in terms of local temperature variations, indicates an increase in sea-surface temperatures of approximately 4°C during isotope stages 11 to 8.

Visual examination of the isotope curve indicates a marked change in amplitude and frequency of the isotope signal at about 80 mbsf. Frequency analyses confirm a major change in frequency of $\delta^{18}O$ values for intervals younger and older than 400 k.y., that corresponds to both a marked temperature change and changes in depositional styles at Site 820. We suggest that these phenomena are related and may have catalyzed the growth of the Great Barrier Reef.

ACKNOWLEDGMENTS

The assistance of Joe Cali at the Research School of Earth Sciences, The Australian National University, and Paul Attenborough at BMR's Marine Sedimentology Laboratory is gratefully acknowledged.

REFERENCES*

Berggren, W.A., Burckle, L.H., Cita, M.B., Cooke, H.B.S., Funnell, B.M., Gartner, S., Hays, J.D., Kennett, J.P., Opdyke, N.D., Pastouret, L.,

* Abbreviations for names of organizations and publication titles in ODP reference lists follow the style given in *Chemical Abstracts Service Source Index* (published by American Chemical Society).

Shackleton, N.J., and Takayanagi, Y., 1980. Towards a Quaternary time scale. *Quat. Res. (N.Y.),* 13:277–302.

Bolli, H.M., and Premoli-Silva, I., 1973. Oligocene to Recent planktonic foraminifera and stratigraphy of the Leg 15 Sites in the Caribbean Sea. *In* Edgar, N.T., Saunders, J.B., et al., *Init. Repts. DSDP,* 15: Washington (U.S. Govt. Printing Office), 475–497.

Broecker, W.S., 1974. *Chemical Oceanography:* New York (Harcourt Brace Jovanovich).

Chappell, J., and Shackleton, N.J., 1986. Oxygen isotopes and sea level. *Nature,* 324:137–140.

Davies, P.J., McKenzie, J.A., Palmer-Julson, A., et al., 1991. *Proc. ODP, Init. Repts.,* 133: College Station, TX (Ocean Drilling Program).

Davies, P.J., Symonds, P.A., Feary, D.A., and Pigram, C.J., 1988. Facies models in exploration: the carbonate platforms of northeast Australia. *APEA J.,* 28:123–43.

————, 1989. The evolution of the carbonate platforms of northeast Australia. *In* Crevello, P.D., Wilson, J.L., Sarg, J.F., Read, J.F. (Eds.), *Controls on Carbonate Platform and Basin Development.* Spec. Publ.—Soc. Econ. Paleontol. Mineral., 44:233–258.

DeMenocal, P.B., Ruddiman, W.F., and Kent, D.V., 1990. Depth of post-depositional remanence acquisition in deep-sea sediments: a case study of the Brunhes-Matuyama reversal and oxygen isotopic Stage 19.1. *Earth Planet. Sci. Lett.,* 99:1–13.

Emiliani, C., 1955. Pleistocene temperatures. *J. Geol.,* 63:539–578.

Epstein, S., Buchsbaum, S.R., Lowenstam, H.A., and Urey, H.C., 1953. Revised carbonate-water isotopic temperature scale. *Geol. Soc. Am. Bull.,* 64:1315–1326.

Feary, D.A., Pigram, C.J., Davies, P.J., Symonds, P.A., Droxler, A.W., and Peerdeman, F., 1990. Ocean Drilling Program—Leg 133—Northeast Australia safety package. *Bur. Miner. Resour. Aust. Rec.,* 1990/6.

Harris, P.T., Davies, P.J., and Marshall, J.F., 1990. Late Quaternary sedimentation on the Great Barrier Reef continental shelf and slope east of Townsville, Australia. *Mar. Geol.,* 94:55–77.

Imbrie, J., 1985. A theoretical framework for the Pleistocene ice ages. *J. Geol. Soc. London,* 142:417–432.

Imbrie, J., Shackleton, N.J., Pisias, N.G., Morley, J.J., Prell, W.L., Martinson, D.G., Hays, J.D., McIntyre, A., and Mix, A.C., 1984. The orbital theory of Pleistocene climate: support from a revised chronology of the marine $\delta^{18}O$ record. *In* Berger, A.L., Imbrie, J., Hays, J., Kukla, G., and Saltzman, B. (Eds.), *Milankovitch and Climate* (Pt. 2): Dordrecht (D. Reidel), 269–305.

Killingley, J.S., Johnson, R.F., and Berger, W.H., 1981. Oxygen and carbon isotopes of single shells of planktonic foraminifera from Ontong-Java Plateau. *Palaeogeogr., Palaeoclimatol., Palaeoecol.,* 33:193–204.

Maasch, K.A., 1988. Statistical detection of the mid-Pleistocene transition. *Clim. Dyn.,* 2:133–143.

Martinson, D.G., Pisias, N.G., Hays, J.D., Imbrie, I., Moore, T.C., Jr., and Shackleton, N.J., 1987. Age dating and the orbital theory of the ice-ages: development of a high-resolution 0 to 300,000-year chronostratigraphy. *Quat. Res. NY,* 27:1–29.

Pickard, G.L., Donguy, J.R., Henin, C., and Rougerie, F., 1977. *A Review of the Physical Oceanography of the Great Barrier Reef and western Coral Sea.* Aust. Inst. Mar. Sci. Monogr. Ser., 2.

Prell, W.L., 1982. Oxygen and carbon isotope stratigraphy for the Quaternary of Hole 502B: evidence for two modes of isotopic variability. *In* Prell, W.L., Gardner, J.V., et al., *Init. Repts. DSDP,* 68: Washington (U.S. Govt. Printing Office), 455–464.

Prell, W.L., Imbrie, J., Martinson, D.G., Morley, J.J., Pisias, N.G., Shackleton, N.J., and Streeter, H.F., 1986. Graphic correlation of oxygen isotope stratigraphy: application to the late Quaternary. *Paleoceanography,* 1:137–162.

Ruddiman, W.F., McIntyre, A., and Raymo, M., 1986. Matuyama 41,000-year cycles: North Atlantic Ocean and northern hemisphere ice sheets. *Earth Planet. Sci. Lett.,* 80:117–129.

Ruddiman, W.F., Raymo, M.E., Martinson, D.G., Clement, B.M., and Backman, J., 1989. Pleistocene evolution: Northern Hemisphere ice sheets and North Atlantic Ocean. *Paleoceanography,* 4:353–412.

Shackleton, N.J., Berger, A., and Peltier, W.R., 1990. An alternative astronomical calibration of the lower Pleistocene time scale based on ODP Site 677. *Trans. R. Soc. Edinburgh, Earth Sci.,* 81:251–261.

Shackleton, N.J., and Hall, M.A., 1989. Stable isotope history of the Pleistocene at ODP Site 677. *In* Becker, K., Sakai, H., et al., *Proc. ODP, Sci. Results,* 111: College Station, TX (Ocean Drilling Program), 295–316.

Shackleton, N.J., and Opdyke, N.D., 1973. Oxygen isotope and paleomagnetic stratigraphy of equatorial Pacific core V28-238: oxygen isotope temperatures and ice volumes on a 10^5 year and 10^6 year scale. *Quat. Res. (N.Y.),* 3:39–55.

Thierstein, H.R., Geitzenauer, K., Molfino, B., and Shackleton, N.J., 1977. Global synchroneity of late Quaternary coccolith datum levels: validation by oxygen isotopes. *Geology,* 5:400–404.

Date of initial receipt: 20 April 1992
Date of acceptance: 8 February 1993
Ms 133SR-288

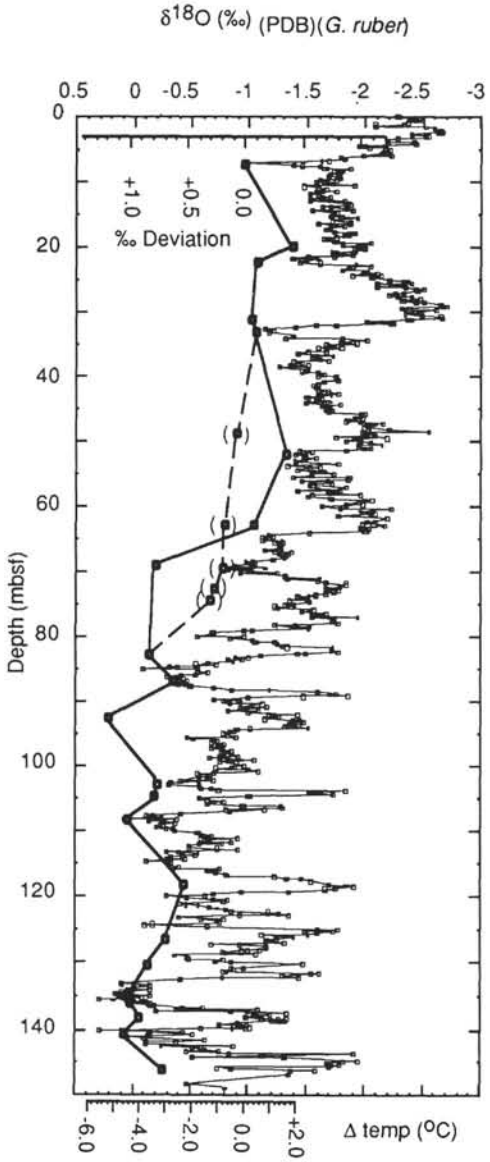

Figure 5. The $\delta^{18}O$ values for Holes 820A and 820B overlain by a bold line that represents the difference in isotopic signature between Hole 677A (Shackleton and Hall, 1989) and Holes 820A and 820B, expressed in per mil deviation and temperature equivalent (at the base of the figure). For the latter conversion, we used 1°C per 0.23‰ $\delta^{18}O$ (Epstein et al., 1953). Dots bounded by parentheses and connected by dotted lines represent calculations for the first age model discussed in the text.

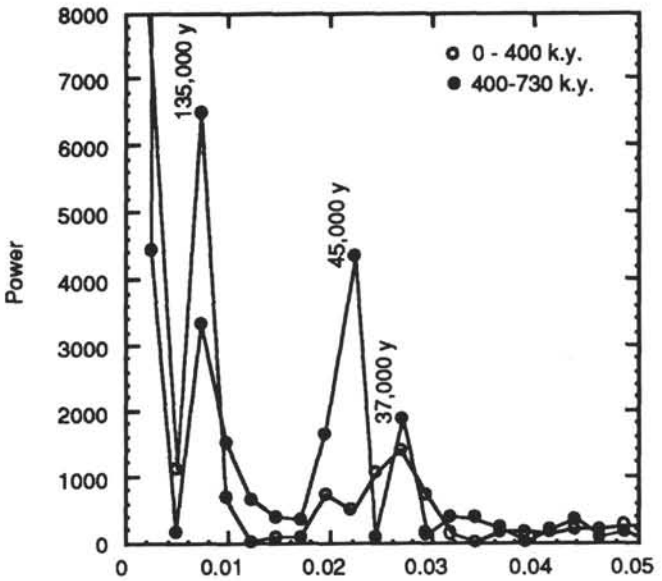

Figure 6. Time-frequency analyses of the oxygen-isotope signal of Holes 820A and 820B for the intervals 0–400 and 400–730 k.y. for the second age model discussed in the text. The isotope-depth signal has been converted into an isotope-time signal using the ages of stage boundaries defined by Imbrie et al. (1984) and by interpolation over 1000-yr increments. The isotope signal from sediments older than 400 k.y. contains dominant frequencies at about 45 and 37 k.y., whereas sediments younger than 400 k.y. have a $\delta^{18}O$ signal with a dominant frequency at 135 k.y.

Table.4 Calculated differences in the $\delta^{18}O$ values between Holes 820A and 820B (Shackleton and Hall, 1989) at equivalent oxygen-isotope stages.

Stages	$\delta^{18}O$ (Hole 677A)	$\delta^{18}O$ (Hole 820A)	Deviation (‰)	Norm. (stage 2) (‰)
2	5.11	–0.97	6.08	0
(3)	4.49	–1.98	6.47	–0.39
(4)	4.75	–1.45	6.20	–0.12
5	3.49	–2.66	6.15	–0.07
6	5.08	–1.13	6.21	–0.13
(7)	3.91	–2.11	6.02	0.06
(7.5)	3.83	–2.09	5.92	0.16
8.4	5.06	–1.45	6.51	–0.43
8.	3.95	–2.20	6.15	–0.07
8.6	4.49	–0.82	5.31	0.77
(8.4)	5.06	–0.82	5.88	0.20
(8.5)	3.95	–1.83	5.78	0.30
(8.6)	4.49	–1.24	5.73	0.35
9	3.47	–1.74	5.21	0.87
10	5.23	–0.25	5.48	0.60
11	3.38	–1.49	4.87	1.21
12	4.95	–0.41	5.36	0.72
13	3.74	–1.60	5.34	0.74
14	4.68	–0.21	4.89	1.19
15.1	3.58	–1.85	5.43	0.65
15.3	3.71	–1.61	5.32	0.76
15.5	3.61	–1.47	5.22	0.86
16	5.16	0.09	5.07	1.01
17	3.64	–1.45	5.14	0.94
18	4.76	–0.28	5.04	1.04
19	3.64	–1.71	5.35	0.73

Note: To obtain the deviation between the two holes, we subtracted the successive $\delta^{18}O$ values for equivalent glacial and interglacial stages of Hole 820A from those of Hole 677A. Values have subsequently been normalized vs. the differential $\delta^{18}O$ value for stage 2. For example,, the $\delta^{18}O$ value for stage 5 in Hole 820A appears to be approximately 0.07‰ greater than the value in Hole 677A and stage 16 is approximately 1.01‰ less. The values bounded by parentheses display calculations for isotopic events as proposed in the first age model discussed in the text.